How finite sample dimensions affect the reversal process of magnetic dot arrays

Ben Van de Wiele, Samuele Fin, Anandakumar Sarella, Paolo Vavassori, and Diego Bisero

Articles you may be interested in

Probing the magnetization reversal process of permalloy nano-rings with high wall height-to-thickness ratios
J. Appl. Phys. **113**, 17B907 (2013); 10.1063/1.4799777

Effect of spatially asymmetric dipolar interactions in the magnetization reversal of closely spaced ferromagnetic nanoisland arrays
J. Appl. Phys. **111**, 07B913 (2012); 10.1063/1.3677269

Lattice symmetry and magnetization reversal in micron-size antidot arrays in Permalloy film
J. Appl. Phys. **91**, 7992 (2002); 10.1063/1.1453321

Magneto-optic Kerr effect investigation of cobalt and permalloy nanoscale dot arrays: Shape effects on magnetization reversal
Appl. Phys. Lett. **77**, 4410 (2000); 10.1063/1.1326841

The magnetic anisotropy and domain structure of permalloy antidot arrays
J. Appl. Phys. **87**, 6322 (2000); 10.1063/1.372693

How finite sample dimensions affect the reversal process of magnetic dot arrays

Ben Van de Wiele,[1] Samuele Fin,[2] Anandakumar Sarella,[3] Paolo Vavassori,[2,3,4] and Diego Bisero[2,5]

[1]*Department of Electrical Energy, Systems and Automation, Ghent University, 9052 Ghent, Belgium*
[2]*Dipartimento di Fisica e Scienze della Terra, Università degli Studi di Ferrara, 44122 Ferrara, Italy*
[3]*CIC nanoGUNE Consolider, Donostia-San Sebastian, Spain*
[4]*IKERBASQUE, Basque Foundation for Science, 48011 Bilbao, Spain*
[5]*CNISM, Unità di Ferrara, 44122 Ferrara, Italy*

We investigate the magnetization reversal of a magnetic dot array by means of magneto-optical Kerr effect and magnetic force microscopy measurements as well as micromagnetic simulations. We find that the finite dimensions of the dot array introduce a global configurational anisotropy that promotes state transitions first in dots near the sample boundaries. From there, the reversal process expands towards the sample body by means of collective magnetization processes originating in the magnetostatic coupling between the dots. These processes are characterized by transition avalanches and the formation of magnetization chains. These findings are important in the development of applications that rely on a robust control of dot magnetization states in dot arrays. © 2014 AIP Publishing LLC. [http://dx.doi.org/10.1063/1.4899138]

Historically, dense arrays of magnetic dots have been studied in the development of magnetic memories, concentrating on a robust control of magnetization states[1] and on finding fast reversal mechanisms in individual dots.[2,3] In the latter, interaction amongst different dots cannot be avoided when interdot distances become smaller than their lateral size.[4–6] More recently, the interactions amongst dots in an array are also regarded useful as collective spin wave properties existing in periodic structures enable the design of magnonic crystals.[7,8] Here, the propagation properties of the spin waves can be tailored by adjusting the periodicity and the material properties of the array. This way, magnonic crystals can be tuned to operate as magnetic waveguides, memories, filters, etc.[9–11] However, the collective spin wave properties are only prominent, if all dots are in an identical magnetization state.[12] Also, arrays of interacting nanomagnets allow the exploration of geometrically induced magnetic frustration and the design of novel metamaterials. Their properties originate in the shape and material properties of the nanomagnets combined with tailored periodic arrangement. Such frustrated systems can lead to new static (logics, info processing) and dynamic (meta-magnonic crystals) properties.[13,14]

Although crucial for applications, in experiments, interdot interactions and finite array dimensions complicate a robust control of the magnetization states. While the shape of the dots (circular, square, etc.) introduces a *configurational anisotropy*,[15–17] we find that the finite array dimensions introduces an additional *global configurational anisotropy*. Both effects originate at the demagnetizing interactions playing at different space scales: the dot and total sample space scale, respectively.

Simulations of dot arrays are often restricted to one dot assuming isolated non-interacting magnetization processes, e.g., when studying reversal processes.[18–21] Periodic boundary conditions are often used to incorporate interdot interactions, still limiting computations to a restricted number of dots and assuming infinite lattice periodicity.[22–25] Then, configurational anisotropy is accounted for, but global configurational anisotropy is not.

In this letter, we show that mutual dot interactions together with finite array dimensions have a non-negligible impact on the magnetization reversal of a dot array. We numerically and experimentally study the hysteresis properties of a Permalloy (Py) array of 16×16 circular dots with thickness of 13 nm and diameter of 315 nm placed on a square grid with 400 nm periodicity. In magneto-optical Kerr effect (MOKE) measurements, in-field magnetic force microscope (MFM) measurements and simulations, we find that global shape anisotropy steers the magnetization reversal of the array: the dots run through different magnetization states depending on the dot location and sample properties and collective magnetization processes occur, leading to transition avalanches and formation of magnetization chains. Moreover, we find that imperfections as edge roughness and external perturbations as the MFM measurement itself anticipate the dots reversal path set by the global configurational anisotropy and promote field induced magnetization state changes.

With electron beam lithography, we drew the dot array patterns on electron sensitive resist layers coated on the Si(100) substrate. Then, a Py layer was deposited at a rate of 0.8 Å/s by electron-beam evaporation. Finally, the resist is removed in a lift-off process. The resulting sample has estimated variations in planar dimensions of ± 10 nm and thickness of 13 ± 1.5 nm. Hysteresis loops were measured using MOKE based on an optical wide-field polarization microscope optimized for Kerr microscopy,[26] while applying arbitrary magnetic fields. To measure the magnetization distribution, MFM images were recorded by a Digital Instruments Nanoscope IIIa, in phase detection mode, monitoring the cantilevers phase of oscillation while the CoCr tip is scanning the sample surface at an average distance of 50 nm (lift mode). Running through the hysteresis loop,

MFM measurements were performed for successive in-plane external fields.

Simulations are performed using MuMax[27] considering in-plane sample dimensions identical to the fabricated sample. The thickness T is varied between 10 nm and 15 nm. Simulations of descending hysteresis branches closely mimic the MOKE and MFM experiment by starting from saturation and reducing the applied field with steps of 1 mT. After every field jump, the magnetization processes are computed for 50 ns. A high damping $\alpha = 1$ ensures that the system is in equilibrium after this time span.[28] Cells of 3.125 nm $\times$ 3.125 nm $\times$ T are used to discretize the sample (2048×2048 cells). A saturation magnetization $M_{sat} = 740 \times 10^3$ A/m, exchange stiffness $A = 1.2 \times 10^{-11}$ J/m, and zero anisotropy is considered.

The experimental hysteresis loop (MOKE) is shown in Fig. 1(a). It is characterized by a steep magnetization change around the coercive field (at about 2 mT) and a very gradual evolution towards saturation in the opposite magnetization direction (ranging from about 5 mT to 20 mT). Figure 1(b) shows simulated hysteresis branches of the dot array with varying thickness. Only the 15 nm thick sample has a similar shape compared to the experimental one, i.e., steep at the coercive field and a gradual evolution towards high saturation. As often found in the comparison between simulated and experimental hysteresis loops,[29–31] the external fields required in the simulations differ about a factor of 2.

To understand the differences in simulated hysteresis branches, Fig. 2 shows the field dependent distribution of the squared average in plane magnetization $\langle M_{xy} \rangle^2 = \langle M_x \rangle^2 + \langle M_y \rangle^2$ of the dots for the three considered sample thicknesses. Concentrating on the 15 nm thick sample, Fig. 2(a), one observes a gradual decrease of the average in-plane magnetization from about 5 mT, indicating the mainly reversible transition to a state visually recognized as the S-state, see Fig. 2(d). Around -4 mT, some dots reverse magnetization to negative saturation, while others transform to the C-state, see Fig. 2(d). The highly irreversible nature of the S- to C-state transition is reflected by the negligibly small number of dots that have intermediate values for $\langle M_{xy} \rangle^2$. Moreover, Fig. 2(a) shows a collective change in magnetization state at the same applied field. Inspection of the dynamic magnetization learns that overcoming the energy barrier separating the S- and C-state in one dot triggers avalanches where the same transition is continued in neighbors dots due to the magnetostatic coupling.

While some C-states transform to the uniform state (down), others go to the vortex state, see Fig. 2(d). Both transitions have no intermediate $\langle M_{xy} \rangle^2$ values, again reflecting their highly irreversible nature. For increasingly negative fields, the vortex cores gradually shift towards the disk edge leading to a growing $\langle m_{xy} \rangle^2$. At about -45 mT, all existing vortex cores are annihilated, ending the reversal of the dot array. Hence, the tailing of the magnetization curves towards large negative fields observed in the MOKE experiment and in simulations with $T = 15$ nm—see Figs. 1(a) and 1(b)—is the signature of vortex formation, vortex core displacement, and expulsion.

In general, the array contains an ensemble of dots in the uniform, S-, C-, and vortex state. The possible state transitions are sketched in Fig. 1(c). While transitions between the uniform and S-state as well as coherent rotations are to a large extent reversible, other transitions are mainly irreversible. They only occur if some energy barrier depending on the material and geometrical parameters is overcome. For instance, Figs. 2(b) and 2(c) show the influence of sample thickness. For simulations with 10 nm and 13 nm sample thickness, only in very few dots, respectively, the energy barriers between the S- and C-state and between C- and vortex state can be overcome. Fewer highly irreversible transitions result in less losses (narrower hysteresis loops), see Fig. 1(b). Moreover, the energy barrier height depends on the dot location, i.e., on the global configurational anisotropy. Figure 3(a) shows how in the 15 nm thick simulated array, at remanent magnetization, dots at the top and bottom row are in the C-state, while the other are still in the S-state. Near the coercive field, S-, C-, and vortex states exist next to each other, see Fig. 3(b). Here, transition avalanches triggered by one dot and continued in neighboring dots form regions and chains of dots with identical magnetization state due to the long range magnetostatic coupling.

The magnetization states and their energy potentials are influenced by geometrical imperfections (e.g., edge roughness, thickness fluctuations, and dot misalignment) and structural disorder (e.g., lattice defects and grain structure). As an example, Fig. 4 shows state distributions taking into account edge roughness obtained by scanning electron microscope imaging (see inset of Fig 4(a)). In simulations with $T = 10$ nm, rough edges enable transitions to the C-state, not observed in the perfect sample, see Fig. 2(c). Also, S-states
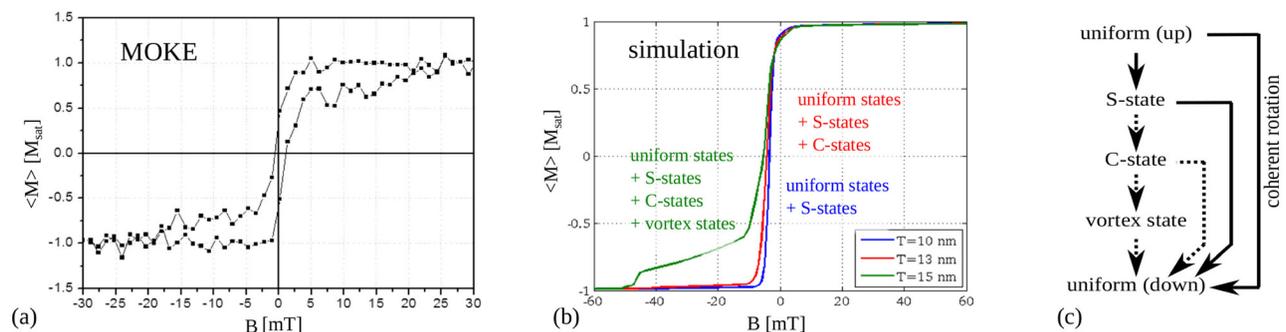

FIG. 1, (a) Dot array hysteresis loop obtained with MOKE. (b) Hysteresis branches simulated with varying sample thickness T. Dots have a perfect circular geometry. With increasing thickness, more magnetization states are observed during reversal. (c) Magnetization states and their transitions: full [dotted] lines represent mainly reversible [highly irreversible] state transitions.
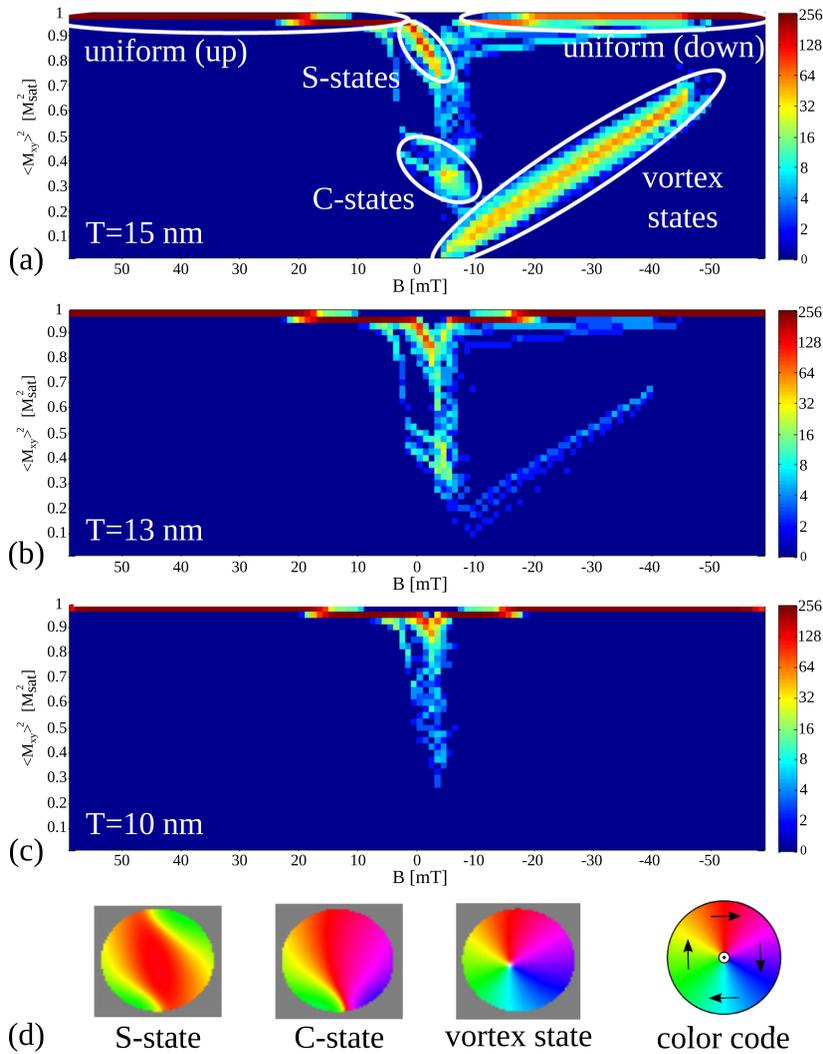
FIG. 2. Distribution of magnetization states when running through the descending hysteresis branch of the dot array simulated with perfectly circular dots and thickness $T = 15$ nm (a), $T = 13$ nm (b), and $T = 10$ nm (c). The y-axes correspond to the square of the average in-plane magnetization of a dot $\langle M_{xy} \rangle^2 = \langle m_x \rangle^2 + \langle m_y \rangle^2$. The colors represent the number of dots in the dot array with a certain in-plane magnetization. (d) Magnetization configuration of a dot in the S-state, C-state, and vortex state, together with the used color code.

are formed earlier. In simulations with $T = 15$ nm, Fig. 4(b), C- and vortex states are reached in more dots and earlier on in the hysteresis loop, compare with Fig. 2(a). Likewise, vortices annihilate at smaller (negative) fields. Other imperfections have similar influence: while the possible magnetization states are set by the dot geometry, array periodicity, and global configurational anisotropy, imperfections change the energy barriers enabling state transitions at different points in the array reversal process which influences the hysteresis loop shape.

Figure 5 shows MFM images of the dot array under successive in-plane external fields. Here, one can only discriminate between vortex and non-vortex states, respectively, recognized as mainly gray with a black or white dot in the center (the vortex core) and a white and/or black color (magnetic charges) at the dot edges. Contrary to the MOKE measurements and simulations where all dots are quasi-uniform for positive fields, the in-field MFM measurement indicates differently: at 6 mT, many vortex states are visible. This seeming discrepancy is due to the stray field of the MFM tip.
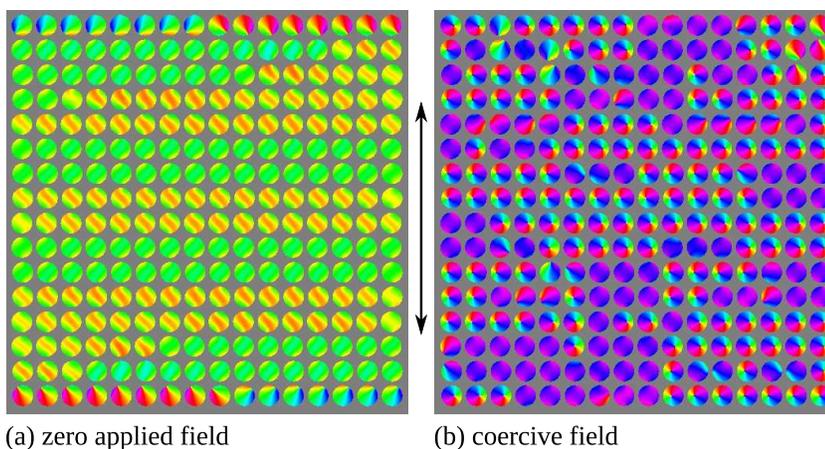

FIG. 3. Magnetization distribution in the dot array simulated with thickness 15 nm at zero applied field (a) and close to the coercive field (b). The color code of Fig. 2(d) is used. The field is applied along the arrows direction from positive saturation (up, green) to negative saturation (down, dark blue).
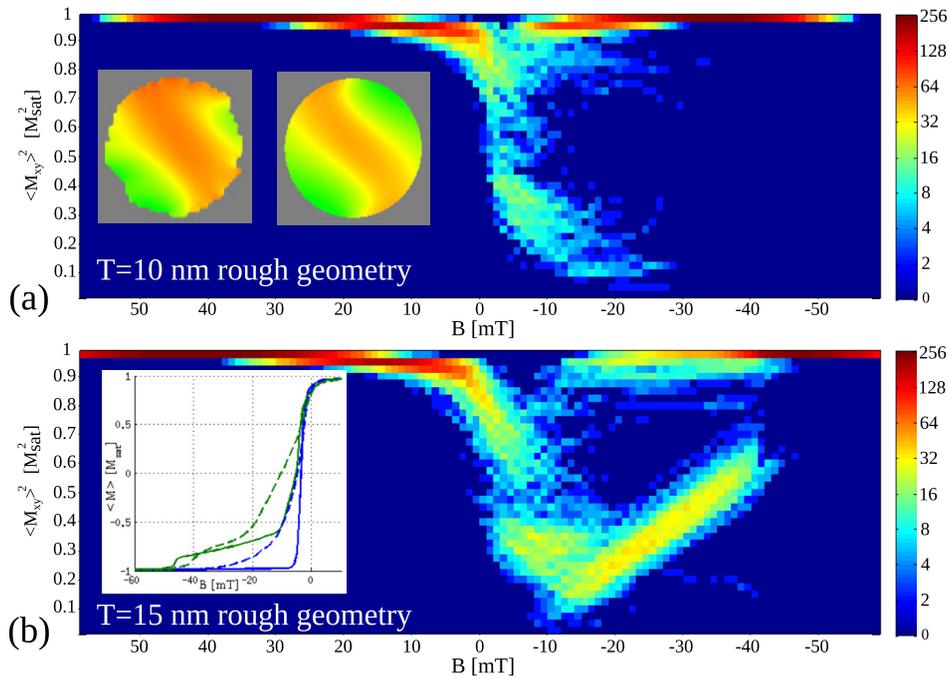
(a) zero applied field   (b) coercive field

FIG. 4. Distribution of magnetization states when running through the descending hysteresis branch of the dot array simulated with thickness $T = 10\,\text{nm}$ (a) and $T = 15\,\text{nm}$ (b) and taking into account edge roughness. The y-axes correspond to the square of the average in-plane magnetization of a dot $\langle M_{xy} \rangle^2 = \langle m_x \rangle^2 + \langle m_y \rangle^2$. The colors represent the number of dots in the dot array with a certain in-plane magnetization. Inset (a): S-state in a dot with rough edges (left) and in a dot with perfect circular geometry (cf. Fig. 2), (b) descending branches for dot array simulated with $T = 10\,\text{nm}$ (blue) and $T = 15\,\text{nm}$ (green), considering perfectly circular dots (full lines) and dots with rough edges (dashed lines).

The MFM tip stray field can add enough energy to facilitate transitions which are unreachable before[32–35] and enable state transitions at different points in the array reversal process, similar to the influence of imperfections. It is, however, clear that the reversal path is mainly set by the local as well as global configurational anisotropy. Indeed, peripheral dots turn to the vortex state at an earlier stage compared to those in the bulk of the array, see Fig. 5 at 6 mT. The panel at 5.3 mT shows how dots in the center revert to the vortex state by means of the nucleation and propagation of magnetization chains parallel to the field direction, a process that already started at 6 mT. Similar behavior has been observed in the magnetization reversal of antidot arrays.[36,37] At zero applied field, all dots are in the vortex state. For increasingly negative fields, one observes the opposite behavior: now centrally located dots are more susceptible to state transitions due to global shape anisotropy. Again, the collective behavior is visible, e.g., at -7.4 mT, where a central chain of neighboring dots made the transition to the uniform state. The MFM images confirm the hysteresis loop asymmetry and the gradual transition to negative saturation, already evidenced by MOKE measurements and simulations. At -10.5 mT, only a fraction of central dots is aligned with the field and at -15.4 mT many peripheral dots did not yet switch to the uniform state, whereas for positive fields the alignment is nearly complete at 8.7 mT. The non-uniformity in magnetization states is observed independent of the tip scanning direction and
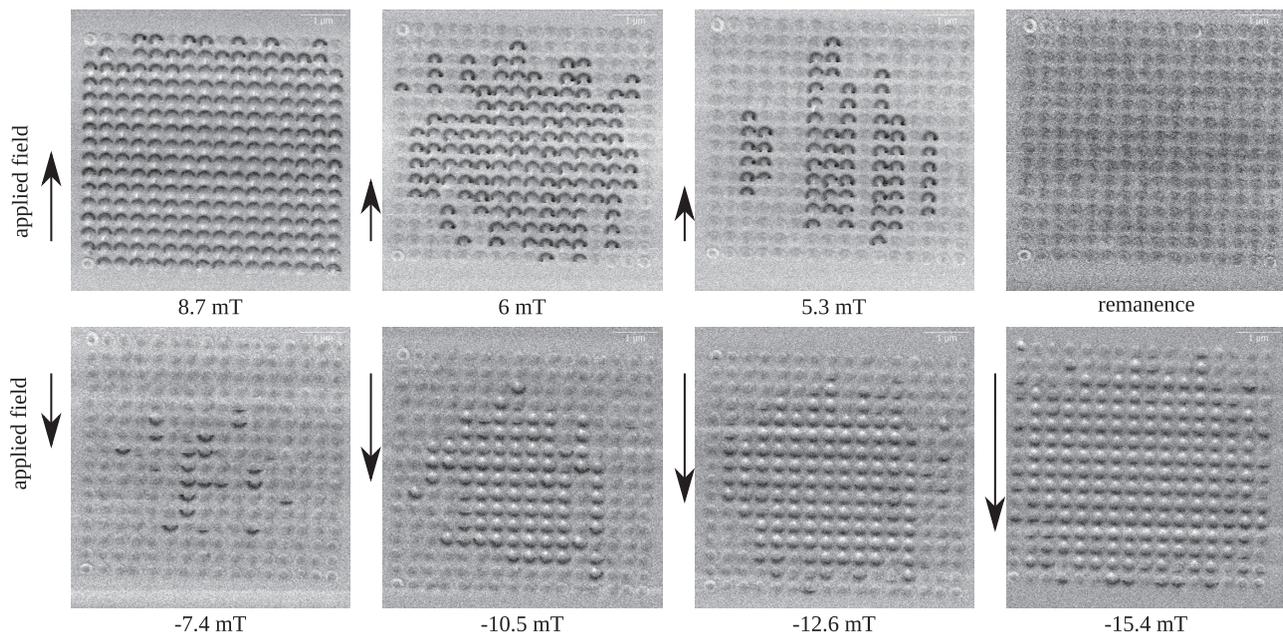

FIG. 5. In-field MFM images measured for successive values of the external field applied in the direction of the arrows.

clearly hints for the existence of transition avalanches observed in simulations.

In the current study, the in-plane array dimensions, $6.4\,\mu m \times 6.4\,\mu m$, were limited by computational restrictions. However, our observations are directly extensible to larger arrays where similar global configurational anisotropy exists and transition avalanches as well as magnetization chains are expected to have even larger sizes. In systems consisting of larger dots, reversal is expected to be even more complex as more metastable equilibrium states exist. In general, the dot array can contain a huge amount of coupled pinned magnetization systems. Therefore, also temperature will have a decisive role as it will also trigger transition events leading to transition avalanches, comparable to creep in magnetic domain wall motion.[38,39] Unfortunately, simulation power is still insufficient to properly address this issue numerically as it requires simulations of large time spans.

In conclusion, we studied the magnetization reversal of a dot array. In simulations as well as experiments, we found that due to the global configurational anisotropy the magnetization reversal first starts at the corners and edges of the dot array and then expands towards the sample body. The reversal is largely determined by collective magnetization processes resulting from the magnetostatic coupling between neighboring dots. In particular, simulations clearly show and MFM experiments strongly hint for the existence of state transition avalanches, e.g., leading to the formation of magnetization chains. Our static observations and dynamic simulations might trigger studies of avalanche-type magnetization processes in dot arrays using dynamical experiments. These are important in the development of magnetic ICT applications relying on the control and/or manipulation of the magnetization state of individual dots within a dot array.

[1]K.-M. Wu, L. Horng, J.-F. Wang, J.-C. Wu, Y.-H. Wu, and C.-M. Lee, Appl. Phys. Lett. **92**, 262507 (2008).

[2]K. Yamada, S. Kasai, Y. Nakatani, K. Kobayashi, H. Kohno, A. Thiaville, and T. Ono, Nat. Mater. **6**, 270 (2007).

[3]M. Kammerer, M. Weigand, M. Curcic, M. Noske, M. Sproll, A. Vansteenkiste, B. Van Waeyenberge, H. Stoll, G. Woltersdorf, C. H. Back, and G. Schuetz, Nat. Commun. **2**, 279 (2011).

[4]K. Y. Guslienko, V. Novosad, Y. Otani, H. Shima, and K. Fukamichi, Phys. Rev. B **65**, 024414 (2001).

[5]G. Gubbiotti, M. Madami, S. Tacchi, G. Socino, G. Carlotti, and T. Okuno, Surf. Sci. **600**, 4143 (2006).

[6]A. Vogel, A. Drews, T. Kamionka, M. Bolte, and G. Meier, Phys. Rev. Lett. **105**, 037201 (2010).

[7]V. V. Kruglyak, S. O. Demokritov, and D. Grundler, J. Phys. D: Appl. Phys. **43**, 264001 (2010).

[8]B. Lenk, H. Ulrichs, F. Garbs, and M. Mnzenberg, Phys. Rep. **507**, 107 (2011).

[9]V. V. Kruglyak, P. S. Keatley, A. Neudert, R. J. Hicken, J. R. Childress, and J. A. Katine, Phys. Rev. Lett. **104**, 027201 (2010).

[10]S. Tacchi, M. Madami, G. Gubbiotti, G. Carlotti, H. Tanigawa, T. Ono, and M. P. Kostylev, Phys. Rev. B **82**, 024401 (2010).

[11]S. Tacchi, F. Montoncello, M. Madami, G. Gubbiotti, G. Carlotti, L. Giovannini, R. Zivieri, F. Nizzoli, S. Jain, A. O. Adeyeye, and N. Singh, Phys. Rev. Lett. **107**, 127204 (2011).

[12]K. Y. Guslienko, J. Nanosci. Nanotechnol. **8**, 2745 (2008).

[13]J. M. Porro, A. Bedoya-Pinto, A. Berger, and P. Vavassori, New J. Phys. **15**, 055012 (2013).

[14]S. Zhang, I. Gilbert, C. Nisoli, G.-W. Chern, M. J. Erickson, L. O'Brien, C. Leighton, P. E. Lammert, V. H. Crespi, and P. Schiffer, Nature **500**, 553 (2013).

[15]R. P. Cowburn and M. E. Welland, Phys. Rev. B **58**, 9217 (1998).

[16]R. P. Cowburn, D. K. Koltsov, A. O. Adeyeye, and M. E. Welland, EPL **48**, 221 (1999).

[17]P. Vavassori, D. Bisero, F. Carace, A. di Bona, G. C. Gazzadi, M. Liberati, and S. Valeri, Phys. Rev. B **72**, 054405 (2005).

[18]A. Thiaville, J. M. Garcia, R. Dittrich, J. Miltat, and T. Schrefl, Phys. Rev. B **67**, 094410 (2003).

[19]J. Sort, A. Hoffmann, S.-H. Chung, K. S. Buchanan, M. Grimsditch, M. D. Baró, B. Dieny, and J. Nogués, Phys. Rev. Lett. **95**, 067201 (2005).

[20]M.-W. Yoo, J. Lee, and S.-K. Kim, Appl. Phys. Lett. **100**, 172413 (2012).

[21]M. Kammerer, H. Stoll, M. Noske, M. Sproll, M. Weigand, C. Illg, G. Woltersdorf, M. Fähnle, C. Back, and G. Schütz, Phys. Rev. B **86**, 134426 (2012).

[22]F. Montoncello and L. Giovannini, Appl. Phys. Lett. **104**, 242407 (2014).

[23]R. Verba, G. Melkov, V. Tiberkevich, and A. Slavin, Appl. Phys. Lett. **100**, 192412 (2012).

[24]A. O. Adeyeye and S. Jain, J. Appl. Phys. **109**, 07B903 (2011).

[25]M. Sepioni, M. Madami, S. Tacchi, G. Gubbiotti, G. Carlotti, D. Bisero, A. O. Adeyeye, N. Singh, and S. Goolaup, J. Phys.: Conf. Ser. **200**, 072089 (2010).

[26]E. Nikulina, O. Idigoras, P. Vavassori, A. Chuvilin, and A. Berger, Appl. Phys. Lett. **100**, 142401 (2012).

[27]A. Vansteenkiste and B. Van de Wiele, J. Magn. Magn. Mater. **323**, 2585 (2011).

[28]We verified in a few cases that by assuming $\alpha = 1$ instead of 0.015 does not alter the reversal process in terms of sequence and structure of the field induced metastable states.

[29]N. Dao, S. R. Homer, and S. L. Whittenburg, J. Appl. Phys. **86**, 3262 (1999).

[30]R. Engel-Herbert, T. Hesjedal, J. Mohanty, D. M. Schaadt, and K. H. Ploog, Phys. Rev. B **73**, 104441 (2006).

[31]K. S. Buchanan, K. Y. Guslienko, A. Doran, A. Scholl, S. D. Bader, and V. Novosad, Phys. Rev. B **72**, 134415 (2005).

[32]S. Landis, B. Rodmacq, and B. Dieny, Phys. Rev. B **62**, 12271 (2000).

[33]X. Zhu, P. Grtter, V. Metlushko, and B. Ilic, Appl. Phys. Lett. **80**, 4789 (2002).

[34]M. Kleiber, F. Kümmerlen, M. Löhndorf, A. Wadas, D. Weiss, and R. Wiesendanger, Phys. Rev. B **58**, 5563 (1998).

[35]J. Lohau, A. Carl, S. Kirsch, and E. F. Wassermann, Appl. Phys. Lett. **78**, 2020 (2001).

[36]B. Van de Wiele, A. Manzin, A. Vansteenkiste, O. Bottauscio, L. Dupré, and D. De Zutter, J. Appl. Phys. **111**, 053915 (2012).

[37]L. J. Heyderman, F. Nolting, D. Backes, S. Czekaj, L. Lopez-Diaz, M. Kläui, U. Rüdiger, C. A. F. Vaz, J. A. C. Bland, R. J. Matelon, U. G. Volkmann, and P. Fischer, Phys. Rev. B **73**, 214429 (2006).

[38]P. Chauve, T. Giamarchi, and P. Le Doussal, Phys. Rev. B **62**, 6241 (2000).

[39]F. Cayssol, D. Ravelosona, C. Chappert, J. Ferre, and J. P. Jamet, Phys. Rev. Lett. **92**, 107202 (2004).